2.A.1:2.I *Nuclear Physics* **A219** (1974) 39—60; © *North-Holland Publishing Co., Amsterdam*


# A STUDY OF THE GIANT DIPOLE RESONANCE OF VIBRATIONAL NUCLEI IN THE $103 \leqq A \leqq 133$ MASS REGION

A. LEPRÊTRE, H. BEIL, R. BERGÈRE, P. CARLOS, A. DE MINIAC and A. VEYSSIÈRE
*C.E.N. Saclay, BP 2, 91190 Gif-sur-Yvette, France*

and

K. KERNBACH
*Erlangen-Nürnberg University, Germany*

Received 13 April 1973
(Revised 8 June 1973)

**Abstract:** This paper presents a set of experimental data concerning the giant dipole resonance of nuclei (GDR) in the $103 \leqq A \leqq 133$ mass region. The cross sections $\sigma(\gamma, n)$ and $\sigma(\gamma, 2n)$ were obtained in the energy region 8–30 MeV by means of a monochromatic photon beam produced by annihilation in flight of positons. This paper attempts also to give an interpretation of the experimental behaviour of the GDR for vibrational nuclei in the $103 \leqq A \leqq 133$ mass region in terms of the simple dynamic collective model. In particular it is shown that the width of the GDR increases as $\beta$ increases and as $E_{2+}$ decreases and that the theoretically predicted spreading of the dipole strength is confirmed by our experimental results. As to the characteristic behaviour of the GDR above its peak value at $E_0$, we come to the conclusion that the actual state of the art in $(\gamma, xn)$ research does not allow one to make an unambiguous choice between isospin splitting or electric quadrupole absorption. Finally the numerical evaluations of the different sum rules are given and some empirical results concerning the average energy of the GDR as a function of $A$ are also presented.

E NUCLEAR REACTIONS $103 \leqq A \leqq 133$ $(\gamma, n)$, $(\gamma, 2n)$, $E = 8$–30 MeV; measured. $\sigma(\gamma, n)$, $\sigma(\gamma, 2n)$; deduced $\sigma(\gamma, tot)$, integrated $\sigma$, Lorentz line parameters, intrinsic quadrupole moments $Q_0$. Natural and enriched targets.

## 1. Available nuclear models

Calculations of the positions and relative strengths of the dipole states of the GDR based on Brown and Bolsterli's [1]) microscopic schematic model, where the initial components are taken to be the simple 1p–1h states, do not exist for heavy nuclei commonly considered to be vibrational ($100 < A < 130$) although they are available for the doubly magic nucleus $^{208}$Pb [refs. [2,3])]. On the other hand, numerical evaluations of sum rules, such as the one of Thomas, Reiche and Kuhn giving the integrated cross section for dipole absorption [4]), were correctly predicted to within a corrective factor taking exchange forces into account.

However a set of predictions concerning the distribution of the dipole strength, capable of giving one some idea as to the evolution of the form of the GDR in the

$100 < A < 130$ mass region, can be obtained from the two following models: (i) the finite Fermi liquid model (FLM); (ii) the dynamic collective model (DCM).

The predictions of the DCM are not only available for most nuclei but are also much easier to apply than those of the FLM since they depend mainly on well known low energy parameters of the nuclei. The DCM was therefore used as the only guide in the interpretation of our experimental results and a brief comparison between the two models will summarize the reasons for this choice.

A study of the interaction between nuclei and electromagnetic fields led Migdal [5]) to propose the finite Fermi liquid theory which was first presented in the form of a semi-classical approximation [6]). Using the same approach, Bunatyan [7]) was able to improve the accuracy of the evaluations of the E1 and E2 resonances in heavy spherical nuclei such as $^{208}$Pb and $^{120}$Sn and Kamerdzhiev [8]) has recently performed the same calculations for the 112, 120 and 124 tin isotopes. These calculations indicate that predicted spreading of the dipole strength depends strongly on the values of the constants $f^{nn}$ and $f^{np}$, where these constants in turn are given by the velocity dependent part of the interaction of identical and different quasi particles, and hence are hardly known experimentally. Moreover, Kamerdzhiev's calculations also show that the evaluated spreading of the dipole strength of $^{112}$Sn and $^{124}$Sn depends to a considerable degree on the inclusion or exclusion of spin-spin forces.

On the other hand, the dynamic collective model (DCM), developed essentially by Le Tourneux [9]) and by Danos and Greiner and their collaborators [10, 11]), simply connects the spreading of the dipole strength to the low energy collective properties which characterize the quadrupole surface vibrations of nuclei:

$$R = R_0[1 + \sum_{\mu} \alpha_{2\mu}(t) Y_{2\mu}(\theta, \phi)]. \tag{1}$$

These vibrational characteristics $\beta$ and $E_{2^+}$ are now experimentally accessible if one measures first the root mean square amplitude of the surface vibrations $\beta$ where

$$\beta^2 = \sum_{\mu} \langle \text{ground state} | \alpha_{2\mu}^2 | \text{ground state} \rangle,$$

$$\beta^2 = \left[\frac{3ZR_0^2}{4\pi}\right]^{-2} B(\text{E2}), \tag{2}$$

and then the energy $E_{2^+}$ of the first $2^+$ excited level corresponding to a one-phonon vibration. The coupling of the dipole oscillations ($H_{\text{dip.}}$ Hamiltonian) and the quadrupole surface vibrations ($H_{\text{quad.}}$ Hamiltonian) is then evaluated in the adiabatic approximation by diagonalizing the total Hamiltonian of the system

$$H = H_{\text{dip.}} + H_{\text{quad.}} + H_{\text{dip. quad.}}$$

in the function space of $H_0 = H_{\text{dip.}} + H_{\text{quad.}}$, and it can be shown that the non-diagonal matrix elements due to the coupling term $H_{\text{dip. quad.}}$ impart a spreading of the dipole strength into several intermediate collective states. An exhaustive study

of just these intermediate collective states as a function of $\beta$ and $E_{2+}$, but considering simple harmonic vibrations only, has been undertaken by Huber [11]), Arenhövel [12]) and Urbas *et al.* [13]). Their results indicate that the spreading ought to increase whenever $\beta$ increases and $E_{2+}$ decreases.

However, there exists no nucleus which is truly a good harmonic spherical vibrator. In particular, recent electron scattering studies of vibrator spectra [14]) have actually connected the form factor observed for $^{110}$Pd, $^{114}$Cd and $^{116}$Sn to the anharmonic vibrator model proposed by Lightbody [15]). A recent improvement of the DCM by Rezwani *et al.* [16]) enabled them to describe any collective behaviour of nuclei in terms of a potential energy surface. This "improved DCM" predicted successfully [17]) the behaviour of the form of the GDR for transition nuclei ($142 < A < 150$), represented by the neodymium isotopes, and recently investigated at Saclay [18]). However, such improved evaluations are not yet available for $100 \lessapprox A \lessapprox 130$ nuclei and this is why, in subsects. 1.1 and 1.2 below, we summarize the predictions concerning the GDR of such $100 \lessapprox A \lessapprox 130$ nuclei as obtained from the original simple DCM when taking harmonic vibrations only into account.

### 1.1. THE TIN ISOTOPES

For these nuclei, the parameters $\beta$ and $E_{2+}$ are practically constant, as can be seen in table 1, and $\beta$ is rather small. Hence it does not come as a surprise that Arenhövel's [12]) calculations predicted a small but essentially constant spreading of the GDR for all tin isotopes as can be seen in fig. 1.

TABLE 1
Low energy parameters $\beta$ and $E_{2+}$ of doubly even Sn isotopes

| | $^{116}$Sn | $^{118}$Sn | $^{120}$Sn | $^{122}$Sn | $^{124}$Sn |
|---|---|---|---|---|---|
| $\beta$ | 0.113 | 0.116 | 0.112 | 0.118 | 0.108 |
| $E_{2+}$ (MeV) | 1.293 | 1.230 | 1.175 | 1.140 | 1.131 |

However, these predictions can not be said to fit the experimental data recently published on the subject and represented in fig. 2 where Fultz *et al.* [19]) find a constant GDR width $\Gamma$ of $4.8 \pm 0.1$ MeV for $^{118}$Sn, $^{120}$Sn and $^{124}$Sn but observes a sudden decrease for $^{116}$Sn where $\Gamma = 4.2$ MeV. He concludes that although $^{116}$Sn does not have a closed neutron shell ($N = 66$), the result of adding valency neutrons to $^{116}$Sn becomes evident through the broadening of the GDR, an effect which is not predicted by the DCM for the Sn isotopes. But Fultz's results are contradicted by a set of data also shown in fig. 2 and recently obtained by Sorokin *et al.* [20]), who used bremsstrahlung photons, and who observed a continuous decrease in $\Gamma$ from 6.2 MeV for $^{116}$Sn to $\Gamma = 4.4$ MeV for $^{124}$Sn.

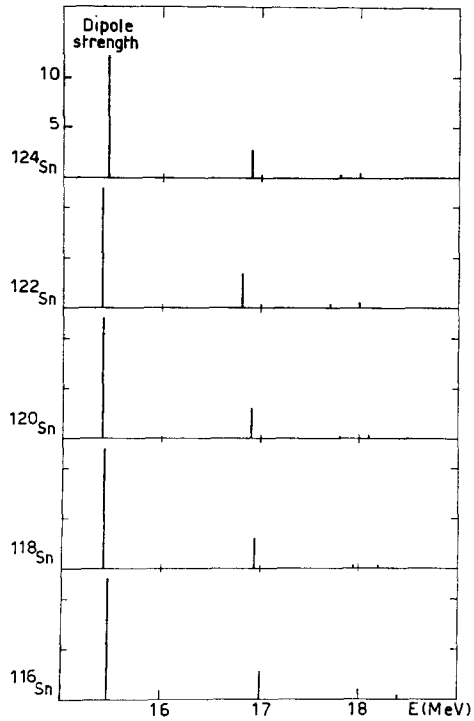


Fig. 1. Spreading of the dipole strength for the tin isotopes as predicted by Arenhövel [12]).

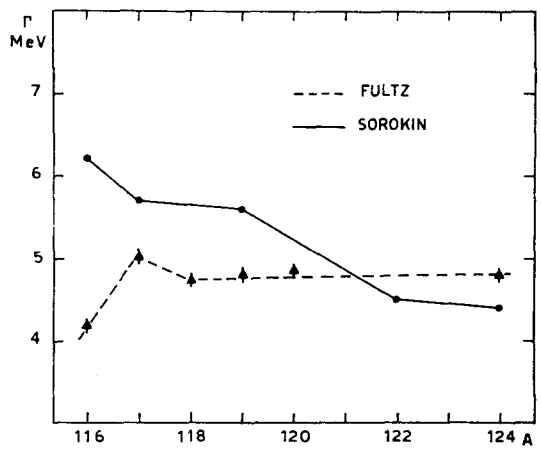


Fig. 2. Experimentally observed GDR widths obtained by Fultz [19]) and Sorokin [20]).

### 1.2. THE Te, Cd AND Pd NUCLEI

A study of the GDR of vibrational nuclei close to the Sn isotopes and for which $\beta$ and $E_{2+}$ are different from the values observed for these Sn isotopes seems also very interesting. Meaningful results, showing a possible correlation with the predictions

TABLE 2

Mean values $\overline{\beta_0}$ and $\overline{E_{2+}}$ of the low energy parameters $\beta$ and $E_{2+}$ for Te, Cd and Pd nuclei

| | Te | Cd | Pd |
|---|---|---|---|
| $\overline{\beta_0}$ | $0.145 \pm 0.018$ | $0.190 \pm 0.010$ | $0.230 \pm 0.020$ |
| $\overline{E_{2+}}$ | $0.750 \pm 0.090$ | $0.580 \pm 0.070$ | $0.460 \pm 0.080$ |
| $E_1 = 78A^{-\frac{1}{3}}$ (MeV) | 15.4 | 16.0 | 16.3 |
| $\beta'_0 = \overline{\beta_0}(\frac{1}{18} E_1)$ | 0.125 | 0.168 | 0.208 |

The $\beta'_0$ and $E_1$ notation is explained in the text.

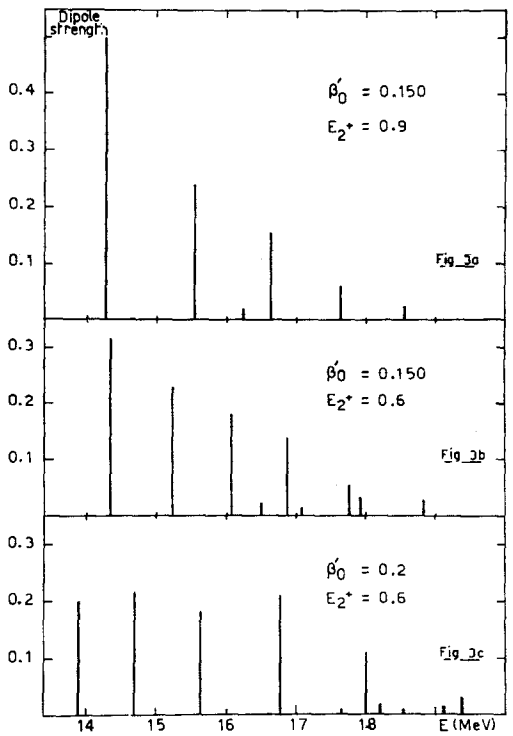


Fig. 3. Theoretical spreading of the dipole strength as computed by Huber [11]) for three typical vibrational nuclei.

of the DCM, can be expected for Te, Cd and Pd nuclei, even with natural targets. For these nuclei, the values of the parameters $\beta$ and $E_{2+}$ for the main isotopes change very little with respect to the mean values $\overline{\beta_0}$ and $\overline{E_{2+}}$ presented in table 2.

Since Huber's calculations on the spreading were performed for $E_1 = 18$ MeV and since $(\beta, E_1)$ is the parameter which contributes most to the spreading, due to the $H_{\text{dip. quad.}}$ coupling, one is obliged to use $\beta'_0 = \overline{\beta_0}(\frac{1}{18}E_1)$ so as to find theoretical

cases as close as possible to the required Te, Cd and Pd nuclei. We thus show in fig. 3 a selection of possible theoretical cases illustrating the spreading of the GDR, each representing as closely as possible, one of the real nuclei Te, Cd and Pd. In particular, fig. 3a shows the results, obtained with $\beta'_0 = 0.150$ and $E_{2+} = 0.9$ MeV, a case which closely resembles tellurium where

$$\frac{\beta'_0}{E_{2+}} = \frac{0.125}{0.750} = \frac{1}{6} = \frac{0.15}{0.90}.$$

In fig. 3b the result shown is for $\beta'_0 = 0.150$ and $E_{2+} = 0.6$ MeV which resembles the cadmium case but with a somewhat smaller theoretically predicted spreading.

In fig. 3c we used $\beta'_0 = 0.2$ and $E_{2+} = 0.6$ MeV, a case which is very similar to palladium but again with a somewhat smaller predicted spreading. If one now compares the prognostications of fig. 1 with those of fig. 3, one observes that about 90% of the dipole strength is concentrated in the following energy intervals $\Delta E$:

$\Delta E = 1.5$ MeV for any of the Sn isotopes;
$\Delta E = 2.2$ MeV for Te (fig. 3a);
$\Delta E = 2.7$ MeV for CD (fig. 3b);
$\Delta E = 4$ MeV for Pd (fig. 3c).

Let us now assume that the damping widths, associated with each of the dipole states which characterize the intermediate collective strengths displayed in figs. 1 and 3, are constant. It then is to be expected that the experimentally observed GDR widths $\Gamma$ will show the following relations:

$\Gamma$ (any Sn isotopes) = constant = $\Gamma$(Sn);
$\Gamma(^{\text{Nat}}\text{Te}) \approx \Gamma(\text{Sn}) + 0.7$ MeV;
$\Gamma(^{\text{Nat}}\text{Cd}) \approx \Gamma(\text{Sn}) + 1.2$ MeV;
$\Gamma(^{\text{Nat}}\text{Pd}) \approx \Gamma(\text{Sn}) + 2.5$ MeV.

Using the quasi-monochromatic photon beam, obtained by means of the annihilation-in-flight technique of monochromatic positons created with the 65 MeV linear accelerator at Saclay [21]), we therefore attempted to verify these predictions for all nuclei discussed in sect. 2 below.

Photoneutrons are detected with a gadolinium loaded liquid scintillator having a high and variable neutron detecting efficiency $40\% < \varepsilon < 60\%$ enabling one to measure the partial photoneutron cross sections $[\sigma(\gamma, \text{n}) + \sigma(\gamma, \text{pn})]$ and $\sigma(\gamma, 2\text{n})$ separately and simultaneously so that the total photoabsorption cross section $\sigma(\gamma, \text{tot}) = \sigma(\gamma, \text{n}) + \sigma(\gamma, \text{pn}) + \sigma(\gamma, 2\text{n})$ becomes directly accessible [22]).

## 2. Experimental investigation of the GDR width

### 2.1. THE TIN ISOTOPES

Characteristics of the samples used are given in table 3.

In fig. 4 we show the partial photoneutron cross sections $[\sigma(\gamma, \text{n}) + \sigma(\gamma, \text{pn})]$ and $\sigma(\gamma, 2\text{n})$ for the different tin isotopes. The error bars in all our experimental results

TABLE 3

Target specifications of Sn isotopes

| | $^{116}$Sn | $^{117}$Sn | $^{118}$Sn | $^{120}$Sn | $^{124}$Sn |
|---|---|---|---|---|---|
| Mass (g) | 50 | 48 | 50 | 50 | 44 |
| Purity (%) | 95.6 | 90.9 | 98.5 | 99.2 | 95.9 |
| Impurities (%) | $^{117}$Sn, 1.9<br>$^{118}$Sn, 1.3 | $^{118}$Sn, 6.5 | | | $^{120}$Sn, 1.45 |

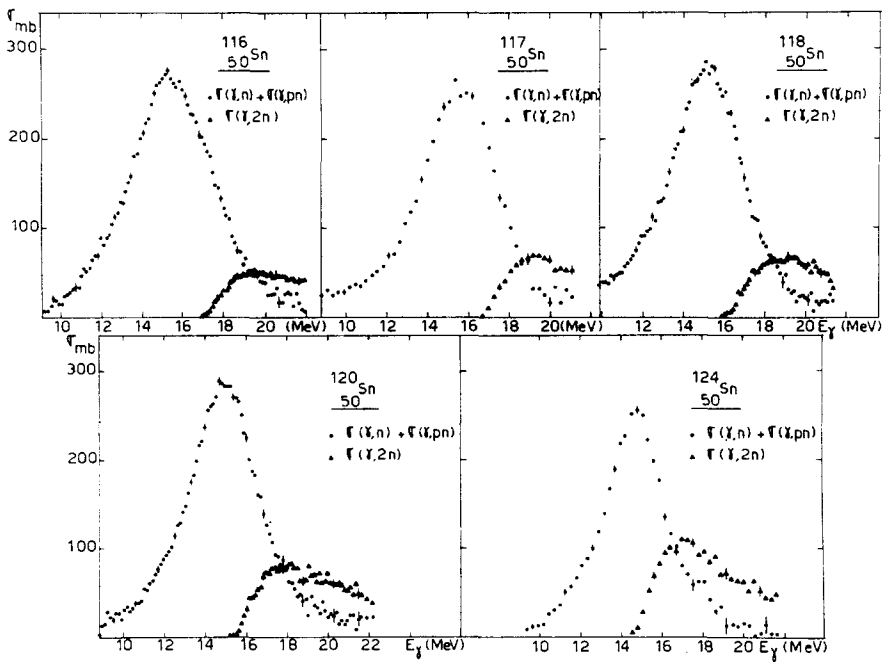


Fig. 4. Partial photoneutron cross sections $[\sigma(\gamma, n)+\sigma(\gamma, pn)]$ and $\sigma(\gamma, 2n)$ for the tin isotopes.

represent statistical errors only but if one takes possible errors in the calibration of the monochromatic photon flux also into account then the absolute error bars at the peak values of the respective GDR are $\approx \pm 20$ mb. One observes that the relative importance of $\sigma(\gamma, 2n)$ increases as one proceeds from $^{116}$Sn towards $^{124}$Sn since its maximum value increases from $\sigma(\gamma, 2n) = 50$ mb to $\sigma(\gamma, 2n) = 110$ mb respectively.

This behaviour of $\sigma(\gamma, 2n)$ is to be expected in view of the fact that the threshold of the $(\gamma, 2n)$ exit channel decreases from $B_{2n} = 17.1$ MeV to $B_{2n} = 14.4$ MeV for $^{116}$Sn and $^{124}$Sn respectively, whereas the average energy $E_1$ of the position of the GDR, namely $E_1 = 78\ A^{-\frac{1}{3}} = 15.5 \pm 0.2$ MeV, remains practically constant for all isotopes concerned. Under these circumstances one ought indeed to observe an

TABLE 4
Lorentz line parameters for a single Lorentz line fit

| | $^{116}$Sn | $^{117}$Sn | $^{118}$Sn | $^{120}$Sn | $^{124}$Sn |
|---|---|---|---|---|---|
| $\sigma_0$ (mb) | 270 | 255 | 278 | 284 | 275 |
| $\Gamma_0$ (MeV) | 5.21±0.1 | 5.30±0.1 | 4.99±0.1 | 5.25±0.1 | 4.96±0.1 |
| $E_0$ (MeV) | 15.57 | 15.67 | 15.44 | 15.38 | 15.29 |

Values of $E_0$ are given to within ±0.1 MeV. Values of $\sigma_0$ are given to within ±5 mb.

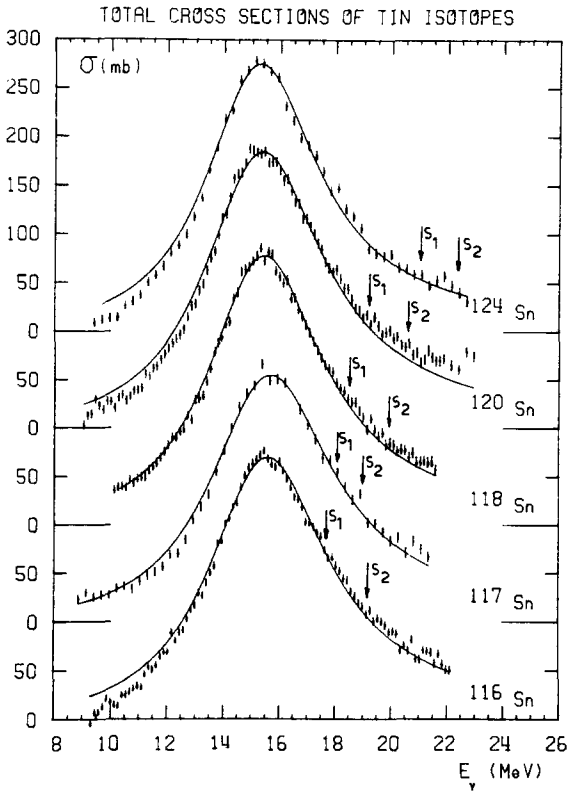


Fig. 5. Best single Lorentz line fit to $\sigma_{exp}(\gamma, \text{tot}) = \sigma(\gamma, \text{n}) + \sigma(\gamma, \text{pn}) + \sigma(\gamma, 2\text{n})$ for the tin isotopes. Arrows $S_1$ and $S_2$ refer to isobaric analogue states as observed by Sugawara [33]) using (e, e'p) reactions.

increase in $\int_{B_{2n}}^{E_{max}} \sigma(\gamma, 2n) dE$ as $B_{2n}$ decreases provided that, upon absorption of a photon, the nucleus in question emits one or two neutrons in cascade as predicted by the statistical model.

Since none of the Sn nuclei possesses a permanent deformation, one can now "fit", according to a standard procedure, a single Lorentz curve $\sigma_L(E)$ to the experimental

TABLE 5

Lorentz line parameters for a two-Lorentz-line fit

| | $E_1$ (MeV) | $\sigma_1$ (mb) | $\Gamma'$ (MeV) | $E_2$ (MeV) | $\sigma_2$ (mb) | $\frac{\sigma_1\Gamma'}{(\sigma_2+\sigma_1)\Gamma'}$ | $\frac{\Sigma_1}{\Sigma_2+\Sigma_1}$ |
|---|---|---|---|---|---|---|---|
| $^{116}$Sn | 15.26 | 222 | 4.54 | 16.72 | 67 | 0.77 | 0.795 |
| $^{118}$Sn | 15.13 | 230 | 4.37 | 16.60 | 68 | 0.775 | 0.775 |
| $^{120}$Sn | 15.04 | 226 | 4.51 | 16.50 | 80 | 0.74 | 0.775 |
| $^{124}$Sn | 14.98 | 230 | 4.10 | 16.44 | 70 | 0.765 | 0.770 |

Errors are the same as in table 4.

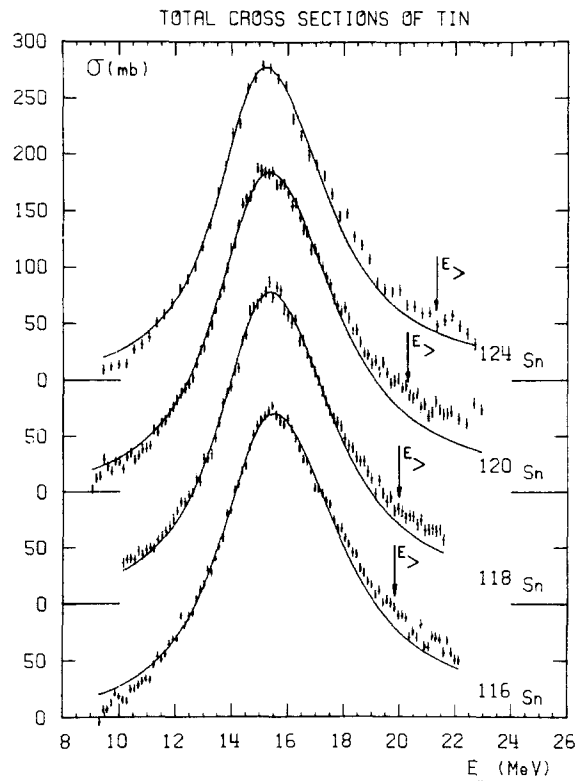


Fig. 6. Best two-Lorentz-line fit to $\sigma_{exp}(\gamma, \text{tot})$ for the tin isotopes where the spacing between the two lines was chosen according to Arenhövel's [12]) computations. The $E_>$ arrows indicate the positions of the $(T+1)$ states as computed by eq. (8).

$\sigma(\gamma, \mathrm{tot})$ results, where it should be kept in mind that a Breit-Wigner type of curve would just as well give satisfactory results [23, 24]):

$$\sigma_L(E) = \sigma_0 \frac{\Gamma_0^2 E^2}{(E^2 - E_0^2)^2 + E^2 \Gamma_0^2} . \tag{3}$$

The resulting Lorentz line parameters for such a fitting process are given in table 4 and the corresponding curves are shown in fig. 5.

As can be seen from fig. 5, reasonable agreement exists in general between the experimental points and the above mathematical expression. However, the fit is not so good for $E > 18$ MeV in $^{120}$Sn and for $E < 13$ MeV in $^{116}$Sn, $^{120}$Sn, and $^{124}$Sn. In particular, one observes that the slope $\mathrm{d}\sigma_L/\mathrm{dE} < \mathrm{d}\sigma_{exp}/\mathrm{dE}$ from 12 to 15 MeV whereas $\mathrm{d}\sigma_L/\mathrm{dE} > \mathrm{d}\sigma_{exp}/\mathrm{dE}$ from 18 MeV onwards. This corresponds to a certain spreading of the dipole strength above $E_0$ which is partly accounted for by a too large $\Gamma_0$ value in the single Lorentz line fit. A better agreement can be obtained if one adjusts two Lorentz lines to the experimental $\sigma(\gamma, \mathrm{tot})$ points, where these two lines are now to be associated with the two main intermediate collective states as calculated by Arenhövel and for which one assumes a constant damping width $\Gamma'$:

$$\sigma'_L(E) = \sigma_1 \frac{E^2(\Gamma')^2}{(E^2 - E_1^2)^2 + E^2(\Gamma')^2} + \sigma_2 \frac{E^2(\Gamma')^2}{(E^2 - E_2^2)^2 + E^2(\Gamma')^2} . \tag{4}$$

Results of such a fit are given in table 5 and fig. 6 where we imposed $E_1 - E_2 = 1.46$ MeV on the fitting process, this condition being predicted by the DCM. It is surprising to note that the average damping width $\Gamma' = 4.4$ MeV is very close to the computed value of 4.6 MeV obtained from the formula $\Gamma^{\downarrow} = 0.027\, E^{1.9}$ established in ref. [24]).

As can be seen from figs. 5 and 6 one obtains a better adjustment between $\sigma_{exp}(\gamma, \mathrm{tot})$ and $\sigma'_L$ [eq. (4)] than between $\sigma_{exp}(\gamma, \mathrm{tot})$ and $\sigma_L$ [eq. (3)], in particular for the rising part of the GDR. This corresponds to the fact that the adjustment parameter $P$ calculated over the $n$ points of the fitting region, from 12 to 18 MeV,

$$P = \frac{1}{n} \sum_{i=1}^{n} [\sigma_{exp}(E_i) - \sigma_L(E_i)]^2,$$

equals 68 for the $^{124}$Sn fit of the GDR with one Lorentz line but only 35 for the two-Lorentz-line fit to eq. (4). Moreover, a remarkable agreement exists between the experimentally observed relative strength of the lower energy state $\sigma_1\Gamma'/[\sigma_1 + \sigma_2]\Gamma'$ and the corresponding theoretical percentage $\Sigma_1/(\Sigma_1 + \Sigma_2)$ predicted by Arenhövel [12]). It can also be seen that $\Gamma' < \Gamma_0$ and that the FWHM value $\Gamma$ of the $\sigma_{exp}(\gamma, \mathrm{tot})$ curve is given by $\Gamma \approx \Gamma_0 = 5.15 \pm 0.15$ MeV for all the Sn isotopes in discrepancy with the continuous decrease of $\Gamma$ with $A$ observed by Sorokin *et al.* [20]) and with the exceptionally low value $\Gamma$ observed for $^{116}$Sn by Fultz *et al.* [19]). Accepting our results and considering that we found $\Gamma_0$ to within $\pm 0.1$ MeV, this can be taken to be a confirmation of the constant value of the spreading of the dipole strength within the framework of the DCM.

## 2.2. THE $_{45}$Rh, $_{46}$Pd, $_{47}$Ag, $_{48}$Cd AND $_{49}$In NUCLEI

All samples used for the $A < 113$ nuclei were composed of natural elements. In fig. 7 we present the partial photoneutron cross sections $[\sigma(\gamma, \mathrm{n})+\sigma(\gamma, \mathrm{pn})]$ and $\sigma(\gamma, 2\mathrm{n})$; the corresponding total cross sections $\sigma_{\mathrm{exp}}(\gamma, \mathrm{tot}) = \sigma(\gamma, \mathrm{n})+\sigma(\gamma, \mathrm{pn})+\sigma(\gamma, 2\mathrm{n})$ are shown in fig. 8. The parameters obtained from a single Lorentz line fit to the $\sigma_{\mathrm{exp}}(\gamma, \mathrm{tot})$ points are given in table 6.

In fig. 8 we again show the actual adjustments made between $\sigma_{\mathrm{L}}$ of eq. (3) and our experimental results $\sigma_{\mathrm{exp}}(\gamma, \mathrm{tot})$ for the above nuclei. It can be seen that $\mathrm{d}\sigma_{\mathrm{L}}/\mathrm{d}E < \mathrm{d}\sigma_{\mathrm{exp}}/\mathrm{d}E$ for $E < 14$ MeV which indicates once again that a single Lorentz line fit does not constitute the ideal adjustment. This is probably due to the fact that the fitting process tries to take the spreading of the dipole strength around $E > E_0$ into account by giving an excessive weighing factor to $\sigma_{\mathrm{L}}$ for $E < E_0$.

The experimental value of the FWHM of the $\sigma_{\mathrm{exp}}(\gamma, \mathrm{tot})$ curve for Ag is

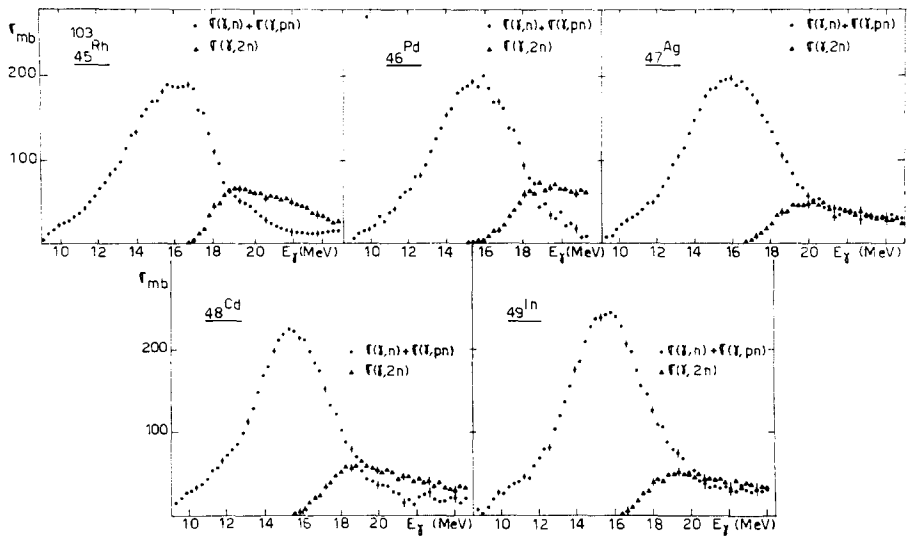


Fig. 7. Partial photoneutron cross sections $[\sigma(\gamma, \mathrm{n})+\sigma(\gamma, \mathrm{np})]$ and $\sigma(\gamma, 2\mathrm{n})$ for $_{45}$Rh, $_{46}$Pd, $_{47}$Ag, $_{48}$Cd and $_{49}$In.

TABLE 6

Lorentz line parameters for a single Lorentz line fit

| | $^{103}_{45}$Rh | $_{46}$Pd | $_{47}$Ag | $_{48}$Cd | $^{115}_{49}$In |
|---|---|---|---|---|---|
| $\sigma_0$ (mb) | 191 | 199 | 198 | 226 | 243 |
| $\Gamma_0$ (MeV) | 7.4±0.1 | 7.1±0.1 | 7.7±0.1 | 6.3±0.1 | 6.1±0.1 |
| $E_0$ (MeV) | 16.15 | 15.9 | 16.1 | 15.8 | 15.8 |

Errors are the same as in table 4.

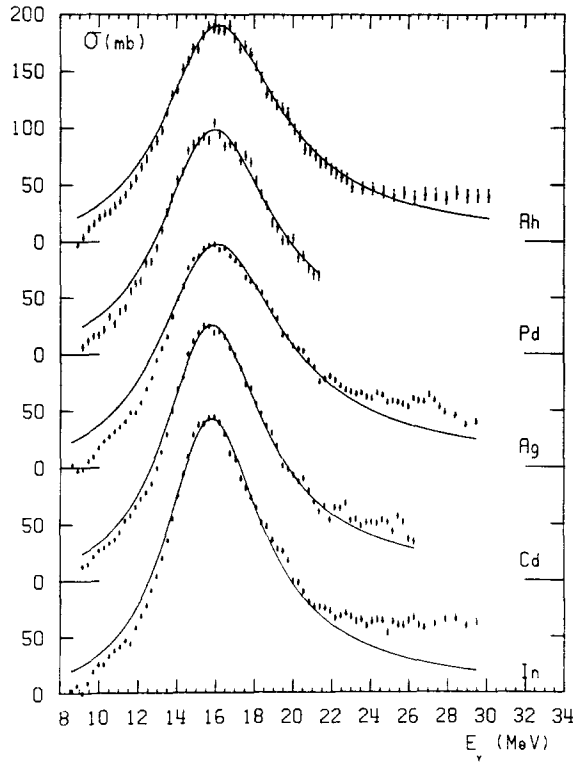


Fig. 8. Best single Lorentz line fit to $\sigma_{exp}(\gamma, \text{tot}) = \sigma(\gamma, \text{n}) + \sigma(\gamma, \text{np}) + \sigma(\gamma, 2\text{n})$ for $_{45}$Rh, $_{46}$Pd, $_{47}$Ag, $_{48}$Cd and $_{49}$In.

$\Gamma = 7.5 \pm 0.15$ MeV which is slightly above the value of 7.0 MeV found by Berman *et al.* [25]) for $^{107}$Ag, whereas our experimental value of $\Gamma = 7.1 \pm 0.15$ MeV, obtained for Pd, is much smaller than the result 8 MeV $< \Gamma <$ 10 MeV which characterizes the $\Gamma$ for the total cross section $\sigma(\gamma, \text{n}) + \sigma(\gamma, \text{np}) + \sigma(\gamma, 2\text{n})$ obtained by Deague *et al.* [26]) with bremsstrahlung photon beams. But since this latter method does not allow a separate measurement of $\sigma(\gamma, 2\text{n})$, this results in large experimental errors for $E > B_{2n}$ thus preventing a precise evaluation of the width $\Gamma$.

As to the rhodium case, Bogdankevitch *et al.* [27]) observed a pronounced splitting of the GDR into two parts, at $E_1 = 14.25$ MeV and at $E_2 = 17.5$ MeV respectively, by unfolding the bremsstrahlung yield data with the Penfold-Leiss method which is known to overemphasize the structures. They ascribed this splitting to the quadrupole deformation of rhodium. However, a two-Lorentz-line fit to our $\sigma_{exp}(\gamma, \text{tot})$ points, with the restriction $\sigma_2\Gamma_2/\sigma_1\Gamma_1 = 2$ corresponding to a prolate deformation imposed on the fitting process, gives an adjustment parameter $P = 13$, for the set of parameters shown in table 7, whereas a one-Lorentz-line fit gave the parameters of table 6 with $P = 17$.

TABLE 7

Lorentz line parameters for a two-Lorentz-line fit of the GDR of rhodium

| $\sigma_1$ (mb) | $E_1$ (MeV) | $\Gamma_1$ (MeV) | $\sigma_2$ (mb) | $E_2$ (MeV) | $\Gamma_2$ (MeV) |
|---|---|---|---|---|---|
| 88 | 15 | 4.94±0.1 | 126 | 17.05 | 6.90±0.1 |

Errors are the same as in table 4.

We can now compute the intrinsic quadrupole moment $Q_0$ of $^{103}_{45}$Rh by means of the classical formulas [4]):

$$0.911d+0.089 = E_2/E_1, \tag{5}$$

$$Q_0 = \tfrac{2}{5}Z(R_0)^2A^{\frac{2}{3}}(d^2-1)/d^{\frac{2}{3}}, \tag{6}$$

which for $R_0 = 1.2$ fm gives $Q_0 = 1.7\pm0.2$ b, a value smaller than the calculated value $Q_0 = 2.2\pm0.1$ b obtained by Heydenburg *et al.* [28]) from their experimental $B$(E2) values using the rotational interpretation.

### 2.3. THE $_{51}$Sb, $_{52}$Te AND $^{133}_{55}$Cs NUCLEI

In fig. 9 we present the partial photoneutron cross sections $[\sigma(\gamma, n)+\sigma(\gamma, pn)]$ and $\sigma(\gamma, 2n)$ with the corresponding total cross section $\sigma_{exp}(\gamma, tot) = \sigma(\gamma, n)+\sigma(\gamma, pn)+\sigma(\gamma, 2n)$ shown in fig. 10. Lorentz line parameters obtained from a single Lorentz line fit to our $\sigma_{exp}(\gamma, tot)$ data are given in table 8 and the best "fits" are also indicated in fig. 10.

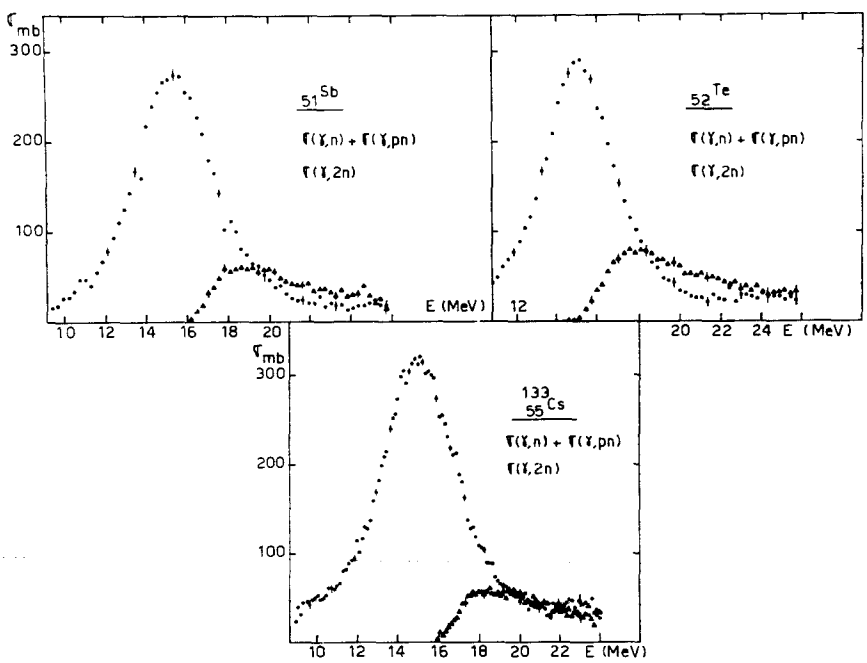


Fig. 9. Partial photoneutron cross sections $[\sigma(\gamma, n)+\sigma(\gamma, np)]$ and $\sigma(\gamma, 2n)$ for $_{51}$Sb, $_{52}$Te and $^{133}_{55}$Cs.

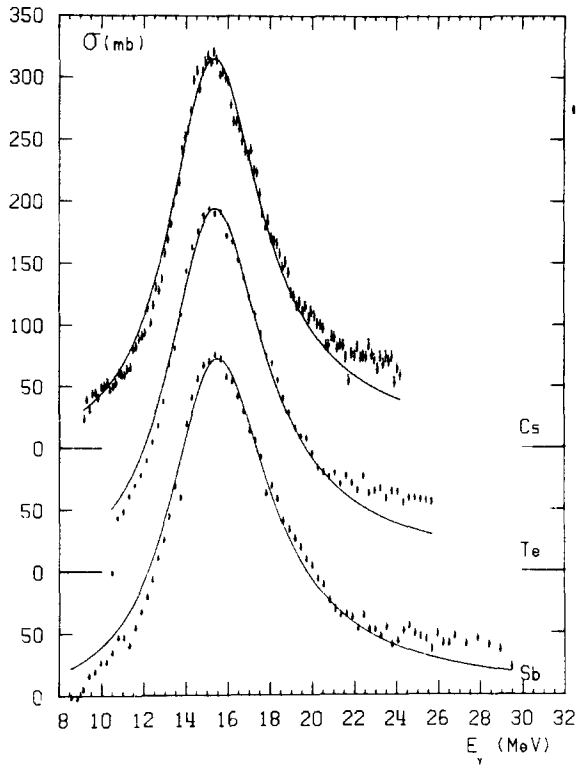


Fig. 10. Best single Lorentz line fit to $\sigma_{exp}(\gamma, \text{tot}) = \sigma(\gamma, \text{n}) + \sigma(\gamma, \text{np}) + \sigma(\gamma, 2\text{n})$ for $_{51}$Sb, $_{52}$Te and $_{55}$Cs.

TABLE 8
Lorentz line parameters for a single Lorentz line fit

| | $_{51}$Sb | $_{52}$Te | $^{133}_{55}$Cs |
|---|---|---|---|
| $\sigma_0$ (mb) | 273 | 294.5 | 315.7 |
| $\Gamma_0$ (MeV) | 5.75±0.1 | 5.49±0.1 | 5.39±0.1 |
| $E_0$ (MeV) | 15.51 | 15.37 | 15.32 |

Errors are the same as in table 4.

As can be seen from fig. 10 such fits are clearly not very good in general since an excess of experimentally observed dipole strength for $16 < E < 20$ MeV is "fitted" only at the expense of a bad adjustment at $E < E_0$. In particular this is quite obvious for the Sb case, whose two isotopes are known to possess oblate deformations and hence possess negative spectroscopic quadrupole moments $Q_s = -0.5$ b and $Q_s = -0.7$ b for $^{121}_{51}$Sb ($I_0 = \frac{5}{2}^+$) and $^{123}_{51}$Sb ($I_0 = \frac{7}{2}^+$) respectively. Hence we tried

to fit our data with two Lorentz lines, where the fitting process is constrained by the imposed characteristic oblate ratio $\sigma_2\Gamma_2/\sigma_1\Gamma_1 = 0.5$. The parameters thus obtained are given in table 9 where it should be noted that the adjustment parameter for such a two-line fit is $P = 51$ whereas $P = 104$ for the Lorentz line parameters given in table 8 and obtained from a single line fit.

TABLE 9

Lorentz line parameters for a two-Lorentz-line fit of the GDR of Sb

| $\sigma_1$ (mb) | $\Gamma_1$ (MeV) | $E_1$ (MeV) | $\sigma_2$ (mb) | $\Gamma_2$ (MeV) | $E_2$ (MeV) |
|---|---|---|---|---|---|
| 217 | 4.17±0.1 | 15 | 96 | 4.72±0.1 | 16.9 |

Errors are the same as in table 4.

Using eqs. (5) and (6) we can now evaluate the intrinsic quadrupole moment of $_{51}$Sb to be $Q_0 = -1.8\pm0.4$ b, a result which shows a surprising agreement with the $Q_0'$ values $-1.4$ b and $-1.5$ b obtained for $^{121}$Sb and $^{123}$Sb respectively and deduced from the simple rotational model formula:

$$Q_0' = \frac{(I_0+1)(2I_0+3)}{I_0(2I_0-1)} Q_s . \tag{7}$$

This could be connected to the fact that Joshi *et al.* [29]) observed a rather strong coupling between the core and the motion of the odd proton for $^{121}$Sb and $^{123}$Sb.

## 2.4. COMMENTS ON THE WIDTH OF THE GDR FOR $100 < A < 133$ NUCLEI

The above experimental results concerning the width of the GDR for quasi-vibrational nuclei allow us to draw the following conclusions;

(a) It is never possible to obtain a very good single Lorentz line fit to $\sigma_{exp}(\gamma, \text{tot})$ but a similar two-line fit gives better results.

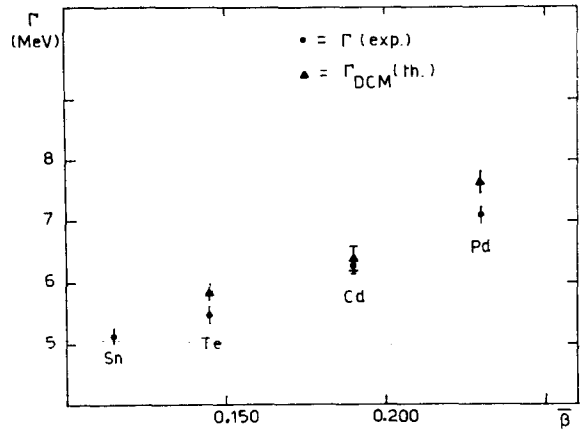


Fig. 11. Comparison between theoretical $\Gamma_{DCM}$ and experimental $\Gamma$ giant dipole resonance widths for Sn, Te, Cd and Pd.

(b) The two main dipole states, computed by Arenhövel within the framework of the DCM for the tin isotopes, are in excellent agreement with the "two-Lorentz-line fits" to our experimental data.

(c) It is possible to find a good two-Lorentz-line fit, corresponding to a prolate and an oblate nuclear deformation for the $^{103}$Rh and Sb nuclei respectively.

Finally, it should be noted that the predictions concerning the spreading of the dipole strength, already discussed in sect. 1, agree to a remarkable degree with the experimentally observed evolution of the width of the GDR, and this in spite of the oversimplified spherical harmonic vibrator model used for such predictions.

In fig. 11 we show the theoretical spreading $\Gamma_{DCM}$ of the GDR of the Te, Cd, and Pd nuclei normalized with respect to the GDR of the Sn isotopes, a result which is in good agreement with our experimental $\Gamma$-values.

## 3. Characteristic behaviour of GDR for $E > E_0$

If one fits the central part of the experimentally obtained GDR with either a single [eq. (3)] or two [eq. (4)] Lorentz lines, one always observes that $\sigma_{exp}(\gamma, \text{tot}) > \sigma_L$ for the high energy tail $E > E_0$ of the GDR. However, the precise amount of such an experimental excess of dipole strength depends to a considerable extent on:

(a) The exactness of $\sigma_{exp}(\gamma, \text{tot})$ which decreases with increasing photon energy because it depends on the accuracy of $\sigma(\gamma, \text{n})$ and $\sigma(\gamma, 2\text{n})$, where the former can become rather bad while the latter remains good in this energy region.

(b) The choice of $\sigma_L$[eq. (3)] or $\sigma'_L$ [eq. (4)] for the fitting process and hence the extrapolation of the GDR to the 20–25 MeV region. By comparing the GDR tails in figs. 5 and 6, one observes indeed that $[\sigma_{exp} - \sigma_L]$ differs appreciably according to the above choice.

Since it is well known that such an excess dipole strength is to be attributed either to the isospin splitting of the dipole absorption [30]) or to an electric quadrupole interaction [13, 31]), we shall now try to identify the physical nature of this experimentally observed excess.

### 3.1. POSSIBLE $(T+1)$ DIPOLE STATES

Dipole states with an isospin $(T+1)$, created when a nucleus with isospin $T$ absorbs a photon by electric dipole absorption E1, can be interpreted, within the schematic representation proposed by Ejiri *et al.* [32]), as being isolated analogue states which interfere with the dipole states of the GDR. Using (e, e'p) reactions, Sugawara *et al.* [33]) observed two such isobaric analogue states (IAS) for each of the Sn isotopes at the energies given in table 10, and referred to by arrows $S_1$ and $S_2$ in fig. 5.

But, contrary to the "structure" observed for $A \approx 90$ nuclei [34]), no similar effect can be clearly distinguished at the corresponding energies of our $\sigma_{exp}(\gamma, \text{tot})$ curves for the Sn isotopes.

The collective dipole mode of isospin $(T+1)$ for $A = 60$ and $A = 90$ has been

TABLE 10
Energies of isobaric analogue states observed by Sugawara [33]) in Sn isotopes, using (e, e'p) reactions

| | $^{116}$Sn | $^{117}$Sn | $^{118}$Sn | $^{120}$Sn | $^{124}$Sn |
|---|---|---|---|---|---|
| Energy of 1st IAS (MeV) | 17.7 | 18 | 18.4 | 19.2 | 21 |
| Energy of 2nd IAS (MeV) | 19.3 | 19 | 19.8 | 20.6 | 22.3 |

predicted [35]) and observed [36]) at an energy $\Delta E$ above the mean energy $E_0$ of the GDR ($\Delta T = 0$), where we have

$$\Delta E \approx 60T/A \text{ MeV}, \tag{8}$$

with a strength obtained from the ratio of the squares of the matrix elements of the dipole transition [30]) given by

$$\frac{|\langle D\rangle_{T+1}|^2}{|\langle D\rangle_T|^2} = \frac{\sigma_{-1}(T+1)}{\sigma_{-1}(T)} = \frac{1}{T+1}\left(1 - \frac{3T}{2A^{\frac{4}{3}}}\right). \tag{9}$$

For $A \approx 90$, eq. (9) gives $\approx 0.10$, which allowed us to observe the $\Delta T = 1$ contribution to the GDR for such nuclei. For the Sn isotopes however, eq. (9) varies from 0.05 to 0.02 for $^{116}$Sn and $^{124}$Sn respectively, and hence the observed differences between $\sigma_{\text{exp}}(\gamma, \text{tot})$ and the best Lorentz fits shown in figs. 5 or 6 are very small at the energies $E_>$ predicted by formula (8). Using ($\gamma$, p) reactions how-

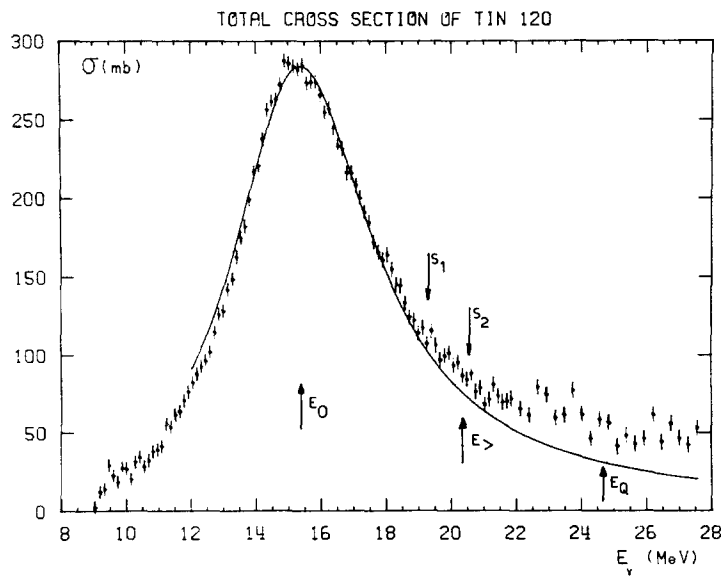


Fig. 12. Typical one-Lorentz-line fit for $^{120}$Sn showing the inherent ambiguity in identifying analogue states $S_1$, $S_2$ and $E_>$ or the E2 state $E_Q$.

TABLE 11
Integrated cross sections

| | $^{103}$Rh | Pd | Ag | Cd | $^{115}$In |
|---|---|---|---|---|---|
| $E_M$ (MeV) | 30 | 21.3 | 29.7 | 26.5 | 29.7 |
| $\sigma_0$ (MeV · b) | 1.75 | 1.38 | 1.90 | 1.75 | 2.1 |
| $0.06\,NZ/A$ (MeV · b) | 1.53 | 1.567 | 1.59 | 1.65 | 1.69 |
| $\sigma'_0/(0.06\,NZ/A)$ | 1.45 | 1.41 | 1.50 | 1.35 | 1.39 |
| $\sigma_{-1}$ (mb) | 96 | 88.2 | 109 | 107 | 121 |
| $\sigma_{-2}$ (mb · MeV$^{-1}$) | 6.2 | 5.8 | 6.6 | 6.8 | 7.4 |
| $\sigma_{-1}/A^{\frac{5}{3}}$ | 0.212 | 0.175 | 0.215 | 0.200 | 0.220 |
| $\sigma_{-2}/A^{\frac{5}{3}}$ | $2.83\times10^{-3}$ | $2.44\times10^{-3}$ | $2.78\times10^{-3}$ | $2.68\times10^{-3}$ | $2.81\times10^{-3}$ |

The average errors $\Delta\sigma_0$ and $\Delta\sigma_0'$ are $\pm0.1$ MeV · mb.

ever, these $(T+1)$ dipole states have recently been observed in $^{124}$Sn by Sorokin [37]) at an energy of 21.6 MeV and with an intensity of 14 MeV · mb as predicted by eqs. (8) and (9) respectively.

### 3.2. POSSIBLE QUADRUPOLE STATES E2

Results obtained at Livermore [19]) were interpreted by Urbas and Greiner [13]) in terms of two dipole states and five quadrupole states. As can be seen from fig. 12, where $^{120}$Sn is given as an example, the excess strength $(\sigma_{exp}(\gamma, \text{tot})-\sigma_L)$ observed at $E_Q \approx 1.6\ E_0 \approx 24.7$ MeV might be interpreted in the above terms, but the experimental accuracies of the real photon absorption technique will have to be improved very much indeed before one can expect a proper identification of these E2 states as has been recently achieved by (e, e') reactions [38–40]).

## 4. Integrated cross sections and sum rules

In table 11 we give the different integrated cross sections defined by

$$\sigma_0 = \int_{E_{Th}}^{E_M} \sigma_{tot}(E)\mathrm{d}E \quad \text{MeV} \cdot \text{b},$$

$$\sigma_{-1} = \int_{E_{Th}}^{E_M} (E^{-1})\sigma_{tot}(E)\mathrm{d}E \quad \text{mb},$$

$$\sigma_{-2} = \int_{E_{Th}}^{E_M} (E^{-2})\sigma_{tot}(E)\mathrm{d}E \quad \text{mb} \cdot \text{MeV}^{-1},$$

$$\sigma'_0 = \tfrac{1}{2}\pi\sigma_1\,\Gamma_1 = \text{area under a single Lorentz line.}$$

Once again we observe that $\sigma_0$ exceeds the classical TRK sum rule $(0.06\,NZ/A)$ as soon as the upper integration limit $E_M$ attains $\approx$ 24 MeV. Furthermore the value of the ratio $(\sigma'_0 A/0.06\,NZ) = 1.3\pm0.15$ confirms once more previously obtained experimental data for heavy nuclei obtained in this laboratory [41, 42]), even if the

as defined in the text

| $^{116}$Sn | $^{117}$Sn | $^{118}$Sn | $^{120}$Sn | $^{124}$Sn | Sb | Te | $^{133}$Cs |
|---|---|---|---|---|---|---|---|
| 29.7 | 21.6 | 23 | 29.7 | 23 | 29.7 | 26 | 24.1 |
| 1.86 | 1.57 | 1.69 | 2.14 | 1.62 | 2.1 | 2.05 | 2.15 |
| 1.71 | 1.72 | 1.73 | 1.75 | 1.79 | 1.78 | 1.85 | 1.93 |
| 1.29 | 1.25 | 1.25 | 1.34 | 1.17 | 1.39 | 1.37 | 1.38 |
| 113 | 102 | 107 | 128 | 104 | 125 | 125 | 136.9 |
| 7.15 | 6.80 | 7.0 | 8.1 | 6.9 | 7.9 | 7.9 | 9.05 |
| 0.203 | 0.181 | 0.188 | 0.220 | 0.171 | 0.210 | 0.198 | 0.205 |
| $2.67\times10^{-3}$ | $2.51\times10^{-3}$ | $2.55\times10^{-3}$ | $2.86\times10^{-3}$ | $2.31\times10^{-3}$ | $2.72\times10^{-3}$ | $2.52\times10^{-3}$ | $2.70\times10^{-3}$ |

single Lorentz line fit to the $\sigma_{exp}(\gamma, \text{tot})$ points does not give an excellent fit. Similarly we found that $\sigma_{-1} \approx (0.2\pm0.02)A^{\frac{1}{3}}$ mb, a value which again agrees with our previous results [41, 42]) but disagrees with the value 0.35 $A^{\frac{1}{3}}$ or 0.3 $A^{\frac{1}{3}}$ mb as computed by Levinger [43]) for an isotropic harmonic oscillator potential and for a finite square potential respectively. Finally, the observed average value $\sigma_{-2} \approx (2.6\pm0.2)A^{\frac{5}{3}}$ mb · MeV$^{-1}$ is also confirmed by our previous data and agrees with the theoretical prediction $\sigma_{-2} \approx 2.25\ A^{\frac{5}{3}}$ as proposed by Migdal [43]).

## 5. The average energy $E_D$ for E1 photon absorption

Within the framework of Steinwedel and Jensen's [44]) interpretation of the collective model proposed by Goldhaber and Teller [45]) applied to the GDR, the restoring force is to be associated with the symmetry energy term $K(N-Z)^2/A$ appearing in the semi-empirical mass formula. This leads one to the following expression for the average E1 absorption energy:

$$E_D = \frac{2.08}{r_0 A^{\frac{1}{3}}} \hbar c \sqrt{\frac{8KNZ}{M^*C^2A^2}} \approx 78A^{-\frac{1}{3}}, \tag{10}$$

where

$M^*$ = effective nucleon mass = $M/(1+\alpha)$;

$r_0A^{\frac{1}{3}} \approx 1.2\ A^{\frac{1}{3}}$ fm = radius of $A(N, Z)$ nucleus;

$\alpha = 0.3$ = coefficient of the exchange term.

The earliest Goldhaber and Teller interpretation, however, supposed the restoring force to be proportional to the nuclear surface area $A^{\frac{2}{3}}$ and since the nuclear mass is proportional to $A$ they found the average E1 absorption energy to be:

$$E_D = C(A^{\frac{2}{3}}/A)^{\frac{1}{2}} = CA^{-\frac{1}{6}}. \tag{11}$$

In fact, eq. (10) does indeed agree reasonably well with the observed evolution of the average energy of the E1 absorption for $A > 100$ nuclei, although eq. (11) is

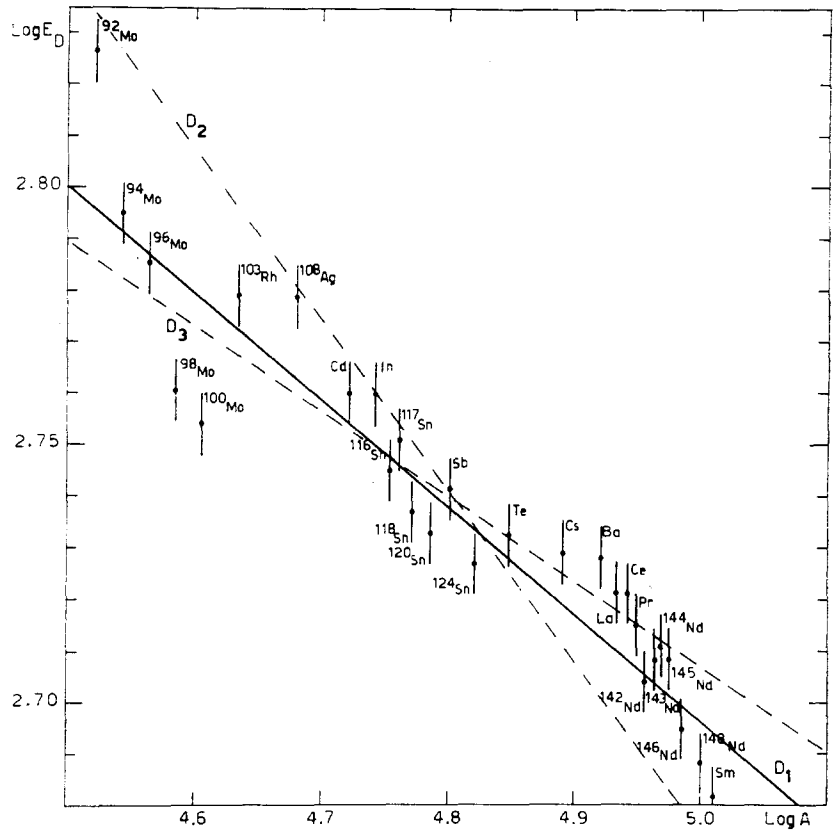


Fig. 13. Experimental results of the average energy $E_D$ of the GDR versus the mass number $A$ with the best fit $E_D = 41.8\, A^{-1/4.8}$ (line $D_1$). Two fits with $A^{-\frac{1}{3}}$ and $A^{-\frac{1}{6}}$ laws are also shown as lines $D_2$ and $D_3$ respectively.

better suited to represent the behaviour of the energy of the maximum of the GDR $E_{max}$ for relatively light nuclei as can be seen from the following example:

$$\frac{E_{max} \text{ for } ^{124}\text{Sn}}{E_{max} \text{ for } ^{28}\text{Si}} = \frac{15.3}{20} \approx \left(\frac{124}{28}\right)^{-\frac{1}{6}}.$$

A new approach to the hydrodynamic model of the GDR, taking the properties of the nuclear surface and in particular its thickness into account, has been proposed by Bach and Werntz [46]), who noted that the Goldhaber-Teller model provides a simple phenomenological expression for the transition density of collective states. This model shows also that an $A^{-\frac{1}{6}}$ behaviour is to be expected for $E_D$. In fig. 13 we present recent data obtained at Saclay for $100 < A < 150$ nuclei, where we have taken the following first approximations as being appropriate for the energy of the

E1 absorption:

$E_D = E_1$ for a single Lorentz line fit,

$E_D = \frac{1}{3}(E_1 + 2E_2)$ for a two-Lorentz-line fit on a prolate nucleus such as $^{150}$Nd.

The best fit for all nuclei making up our experimental data is given by $E_D = 41.8\ A^{-1/4.8}$, designated by the straight line ($D_1$) in fig. 13, which lies between $A^{-\frac{1}{3}}$ of eq. (10) and $A^{-\frac{1}{6}}$ of eq. (11). This intermediate result could possibly be connected to the recent "three-fluid hydrodynamic model" of the GDR proposed by Mohan *et al.* [47]) in which deviations from the $A^{-\frac{1}{3}}$ law should be expected if the $A$-dependence of the parameter $K$, defining the restoring energy densities, is also taken into account.

By imposing restraints $A^{-\frac{1}{3}}$ and $A^{-\frac{1}{6}}$ on the above fitting process one obtains the straight lines $D_2$ and $D_3$ described respectively by

$$E_D = 76.8A^{-\frac{1}{3}}\ \text{MeV},$$

$$E_D = 34.5A^{-\frac{1}{6}}\ \text{MeV},$$

and which are also shown in fig. 13. Finally one can also see, from fig. 13, that for each of the three isotope sets Sn, Nd and Mo, the $A^{-\frac{1}{3}}$ law is closer to the experimental data than the $A^{-\frac{1}{6}}$ expression.

We are greatly indebted to Dr. H. Arenhövel for his calculations on the Sn isotopes and we also wish to thank the USSR Bureau of Isotopes for lending us the isotopes concerned.

## References

1) G. E. Brown and M. Bolsterli, Phys. Rev. Lett. **3** (1959) 4272
2) V. Gillet, A. M. Green and E. A. Sanderson, Nucl. Phys. **88** (1966) 321
3) T. S. Kuo, J. Blomqvist and G. E. Brown, Phys. Lett. **31B** (1970) 93
4) E. Hayward, in Nuclear structure and electromagnetic interactions (Oliver and Boyd, Edinburgh, 1965)
5) A. B. Migdal, The theory of finite Fermi systems, Nanka, 1965
6) A. B. Migdal, A. A. Lushnikov and D. F. Zaretsky, Nucl. Phys. **66** (1965) 193
7) G. G. Bunatyan, Sov. J. Nucl. Phys. **4** (1967) 659
8) S. P. Kamerdzhiev, Yad. Fiz. **15** (1972) 676
9) J. Le Tourneux, Phys. Lett. **13** (1964) 325
10) M. Danos and W. Greiner, Phys. Lett. **8** (1964) 113
11) M. G. Huber, M. Danos, H. J. Weber and W. Greiner, Phys. Rev. **155** (1967) 1073
12) H. Arenhövel, private communication
13) T. D. Urbas and W. Greiner, Phys. Rev. Lett. **24** (1970) 1026
14) S. Penner *et al.*, Proc. Conf. on nuclear structure studies using electron scattering and photoreactions, Sendai, September 1972
15) W. Lightbody, Phys. Lett. **38B** (1972) 475
16) V. Rezwani, G. Gneuss and H. Arenhövel, Nucl. Phys. **A180** (1972) 254
17) V. Rezwani *et al.*, Proc. Conf. on nuclear structure studies using electron scattering and photoreactions, Sendai, September 1972
18) P. Carlos, H. Beil, R. Bergère, A. Leprêtre and A. Veyssière, Nucl. Phys. **A172** (1971) 437
19) S. C. Fultz, B. Berman, J. Caldwell, R. Bramblett and M. Kelly, Phys. Rev. **186** (1969) 1255

20) Y. Sorokin, V. Kruchev and B. Youriev, Izv. Akad. Nauk SSSR **36** (1972) 180
21) G. Audi, N. de Botton, G. Tamas, H. Beil, R. Bergère and A. Veyssière, Nucl. Instr. **79** (1970) 203
22) H. Beil, R. Bergère and A. Veyssière, Nucl. Instr. **67** (1969) 293
23) C. B. Dover, R. Lemmer and F. Hahne, Ann. of Phys. **70** (1972) 458
24) P. Carlos, to be published
25) B. L. Berman, R. L. Bramblett, J. T. Caldwell, H. S. Danis, M. A. Kelly and S. C. Fultz, Phys. Rev. **177** (1969) 1745
26) T. K. Deague, E. G. Muirhead and B. M. Spicer, Nucl. Phys. **A139** (1969) 501
27) O. V. Bogdankevitch, B. I. Goryachev and V. A. Zapevalov, JETP (Sov. Phys.) **15** (1962) 1044
28) N. P. Heydenburg and G. M. Temmer, Phys. Rev. **95** (1954) 861
29) M. C. Joshi and B. Herskind, Proc. Int. Conf. on nuclear structure, Gatlinburg (Academic Press, N.Y., 1967) p. 357
30) S. Fallieros, B. Goulard and R. H. Venter, Phys. Lett. **19** (1965) 398
31) R. Ligensa and W. Greiner, Nucl. Phys. **A92** (1967) 673
32) H. Ejiri and P. Bondorf, Phys. Lett. **28B** (1968) 304
33) M. Sugawara, K. Shoda, T. Saito, H. Miyase, A. Suzuki, S. Oikawa and R. Bergère, Phys. Rev. **C5** (1972) 1705
34) A. Leprêtre, H. Beil, R. Bergère, P. Carlos, A. Veyssière and M. Sugawara, Nucl. Phys. **A175** (1971) 609
35) R. Akyüz and S. Fallieros, Phys. Rev. Lett. **27** (1971) 1016
36) P. Paul, J. Amann and K. Snover, Phys. Rev. Lett. **27** (1971) 1013
37) Y. Sorokin, V. Krushev and B. Yur'ev, Sov. Nucl. Phys. **14** (1972) 622
38) Y. Torizuka *et al.*, Proc. Conf. on nuclear structure studies using electron scattering and photon absorption, Sendai, September 1972
39) S. Fukuda and Y. Torizuka, Phys. Rev. Lett. **29** (1972) 1109
40) F. Busbirk, H. D. Graf, R. Pitthan, H. Theissen, O. Titze and Th. Walcher, Phys. Lett. **42B** (1972) 194
41) R. Bergère, H. Beil, P. Carlos and A. Veyssière, Nucl. Phys. **A133** (1969) 417
42) A. Veyssière, H. Beil, R. Bergère, P. Carlos and A. Leprêtre, Nucl. Phys. **A159** (1970) 561
43) J. S. Levinger, in Nuclear photodisintegration (Oxford University Press, 1960)
44) H. Steinwedel and J. Jensen, Z. Naturf. **5a** (1950) 413
45) M. Goldhaber and E. Teller, Phys. Rev. **74** (1948) 1046
46) R. Bach and C. Werntz, Phys. Rev. **173** (1968) 958
47) R. Mohan, M. Danos and L. C. Biedenharn, Phys. Rev. **C3** (1971) 1740